
GRAPHS GENERALIZATION UNDER DISTRIBUTION SHIFTS

Qin Tian
Tianjin University
Tianjin, China
tianqin123@tju.edu.cn

Wenjun Wang
Tianjin University
Tianjin, China
wjwang@tju.edu.cn

Chen Zhao*
Baylor University
Waco, Texas, USA
chen_zhao@baylor.edu

Minglai Shao†
Tianjin University
Tianjin, China
shaom1@tju.edu.cn

Wang Zhang
Tianjin University
Tianjin, China
wangzhang@tju.edu.cn

Dong Li
Tianjin University
Tianjin, China
ld2022244154@tju.edu.cn

ABSTRACT

Traditional machine learning methods heavily rely on the independent and identically distribution (*i.i.d*) assumption, which imposes limitations when the test distribution deviates from the training distribution. To address this crucial issue, out-of-distribution (OOD) generalization, which aims to achieve satisfactory generalization performance when faced with unknown distribution shifts, has made a significant process. However, the OOD method for graph-structured data currently lacks clarity and remains relatively unexplored due to two primary challenges. Firstly, distribution shifts on graphs often occur simultaneously on node attributes and graph topology. Secondly, capturing invariant information amidst diverse distribution shifts proves to be a formidable challenge. To overcome these obstacles, in this paper, we introduce a novel framework, namely Graph Learning Invariant Domain genERation (GLIDER). The goal of it is to (1) diversify variations across domains by modeling the potential seen or unseen variations of attribute distribution and topological structure, and (2) minimize the discrepancy of the variation in a representation space where the target is to predict semantic labels. Technically, GLIDER consists of three stages. In the first stage, a graph (G') is generated from the original graph (G) by only changing the distribution of node attributes. Then, GLIDER generates multiple graphs (G'') in synthetic domains from G' , wherein node attributes stay the same but topological structure changes in each G'' . Finally, the framework minimizes the semantic gap for each class between G and G'' by learning a domain-invariant classifier. We validate the effectiveness of GLIDER by conducting empirical studies on four real-world graph datasets. Extensive experiment results indicate that our model outperforms baseline methods on node-level OOD generalization across domains in distribution shift on node features and topological structures simultaneously.

1 Introduction

In recent years, out-of-distribution (OOD) generalization has gained prominence as an approach to enhance the performance of machine learning methods when confronted with unknown distributions [1]. The goal of OOD generalization is to find a predictor that is trained using data drawn from a family of related training domains and then evaluated on a distinct and unseen test domain [2]. Indeed, numerous studies have demonstrated the effectiveness of OOD generalization methods on Euclidean data, such as images or molecules that satisfy the *i.i.d* assumption. However, graph-structured data, prevalent in real-world applications, has garnered comparatively less attention despite its substantial importance in high-stakes graph applications. These applications include but are not limited to, molecule prediction [3], financial analysis [4], and criminal justice [5]. For example, social networks consist of users (nodes) who interact with each other and influence each other's behaviors (labels). The structure of these interactions highly

*This work is supervised by Chen Zhao.

†Corresponding author

depends on when and where data is collected. The goal of OOD generation on graphs is to achieve stable and accurate prediction when distribution shifts occur on graph-structured data with complex intrinsic connections.

Due to the incorporation of distribution variations with diverse characteristics in graph-structured data, two main challenges arise: (1) Distribution shifts on the graph can manifest simultaneously in both node attributes and topology, resulting in a substantial and intricate variation. (2) Consequently, the variation poses challenges in capturing invariant information across different domains. Several efforts have been conducted to alleviate these problems by enriching the distribution of the training domain. These methods can be broadly categorized into three types: structure-wise, feature-wise, and mixed-type methods. Structure-wise methods [6, 7] primarily focus on generating a greater variety of training topologies to cover some potential unobserved testing topologies. Feature-wise methods [8, 9] are devoted to generating a more diverse distribution of training attribute features. These two types of methods specifically characterize distribution shifts either in node attributes or graph topologies. Moreover, while mixed-type methods [10, 11] are introduced, these approaches primarily concentrate on graph-level tasks rather than node-level classification. Node-level tasks are essential for capturing the local structures, features, and connections of individual nodes, often relying on information from nearby nodes or edges. Nevertheless, graph-level tasks fail to take these factors into account, rendering them inappropriate for direct implementation in node-level tasks.

In response to the mentioned challenges and limitations, in this paper, we propose a principled framework, namely Graph Learning Invariant Domain genERation (GLIDER), to address the OOD generalization problem for node-level classification on graphs. Graph augmentation in GLIDER contains two steps: (1) $G \rightarrow G'$: the distribution shift only occurs on the attribute matrix, but the topology structure remains, (2) $G' \rightarrow G''$: the distribution shift occurs on topology solely. Specifically, in the initial step, the attribute of each node is disentangled into two factors in latent spaces: a domain-invariant semantic factor and a domain-specific variation factor. By recombining semantic factors with randomly sampled variation factors for all nodes in a graph $G = (A, X)$, a novel graph $G' = (A, X')$ is obtained, where the node attributes X' are generated from X in G but the adjacency matrix remains unchanged. In the second step, we augment the topology through adversarial training. Subsequently, a graph with distribution shift on both the node attribute matrix and topology, denoted as $G'' = (A', X')$, is generated. Finally, GLIDER learns the domain-invariant classifier for node label prediction by minimizing the empirical risk from multiple domains. Our contributions are summarized as follows:

- We introduce a domain generalization framework for node-level tasks on graphs that simultaneously addresses distribution shifts in both attributes and topology. This approach aligns more closely with real-world graph data, offering a more comprehensive and realistic solution.
- We diversify the variation by modeling unseen variations in node attribute distribution and graphic topology. Furthermore, we minimize the semantic gap for each class by reducing the discrepancy of the variation in the representation space to learn the invariant information of nodes across domains.
- We conduct a set of comprehensive experiments on diverse real-world datasets for the node-level prediction task. Our results demonstrate the effectiveness of GLIDER compared to state-of-the-art baselines.

2 Related Works

Out-of-distribution (OOD) Generalization aims to find a trained predictor using data drawn from a family of related training domains and then evaluated on a distinct and unseen test domain [2]. Methodologically, OOD generalization algorithms can be broadly categorized into disentangled representation [12, 13], causal representation [14, 15], domain generation [16, 17], the combination of causal learning and invariant learning [18, 19, 20] and stable learning [21, 22]. Disentangled representation aims to learn representations that effectively separate relevant information factors from irrelevant ones. Domain generalization aims to learn models with strong generalization performance on unpredictable target domains by leveraging multiple source domains with diverse distributions. Following similar spirits, we minimize prediction variance across domains to capture invariant features but do not assume that the source domain comes from multiple environments.

OOD Generalization on Graphs. Despite extensive studies documenting success in addressing the OOD problem for Euclidean data, such as images or molecules, there has been relatively little attention given to graph-structured data, which is prevalent in real-world scenarios. Recently, several graph enhancement methods for OOD generation on graphs have been introduced, which can be broadly categorized into three types: structure-wise augmentations [6, 23], feature-wise augmentations [8, 9], and mixed-type augmentations [10, 11]. Structure-wise augmentations aim at generating a greater variety of training topologies to cover some potential unobserved testing topologies. Feature-wise augmentations are devoted to generating more diverse training attribute feature distribution. The two methods described above solely consider a single type of distribution shift in isolation. Indeed, in real-world scenarios, it is common for both attribute and topology shifts to occur simultaneously in graph-structured data. Further, augmentation methods that

consider both attributes and topology are proposed, but these methods are for graph-level tasks and are not suitable for node-level. This limitation implies that there is scope for additional research or the creation of supplementary techniques to handle node-level issues on graph data.

3 Preliminaries

All notations used in this paper are listed in Table 4 of Appendix A.1.

3.1 Problem Setting and Formulation

Denote a graph $\mathcal{G} = \{G^e\}_{e=1}^{|\mathcal{E}|}$, where $G^e = (A^e, X^e)$ is a subgraph with labels $\mathcal{Y}^e = \{y_v^e\}$ collected from the domain $e \in \mathcal{E}$ and \mathcal{E} denotes the set of domains. It is worth noting that we abuse this notation and all domains share the same label space. $A^e \in \mathbb{R}^{|\mathcal{V}^e| \times |\mathcal{V}^e|}$ denotes the adjacency matrix and $X^e \in \mathbb{R}^{|\mathcal{V}^e| \times d}$ denotes the node attribute matrix, where $|\mathcal{V}^e|$ is the number of nodes and d is the dimension of node feature. The distributions of node attributes and topology in subgraphs vary across domains.

The goal of node-level OOD generation on graphs is to improve the model’s generalization ability for node label prediction across domains. To mitigate the challenges outlined in Section 1, we introduce the ego-graphs for each node $v \in \mathcal{V}$, capturing the surrounding influences on the centered node. We define the node’s ego-graph as $G_v^e = (A_v^e, X_v^e)$, where A_v^e denotes the adjacency matrix and X_v^e denotes the node feature matrix of the ego-graph for node $v \in \mathcal{V}^e$ in domain $e \in \mathcal{E}$. An ego-graph G_v^e of a node includes the center node (ego) v and its L -hop neighbors, where L is an arbitrary integer. The set of edges comprises all the edges present in the ego-graph of these nodes. Naturally, a graph will consist of a series of instances $\{(G_v^e, y_v^e)\}_{v=1}^{|\mathcal{V}^e|}$, where y_v^e denotes the class label of the node v .

Problem 1 (Node-Level OOD Generalization on Graphs). *Let $\mathcal{E}_{train} \subsetneq \mathcal{E}$ be a finite subset of training domains, and assume that for each $e \in \mathcal{E}_{train}$, we have access to a subgraph $G^e = (A^e, X^e)$, and the corresponding $\{(G_v^e, y_v^e)\}_{v=1}^{|\mathcal{V}^e|}$ sampled i.i.d from $\mathbb{P}(G^e, Y^e)$, where $G_v^e = (A_v^e, X_v^e)$. Given a function class \mathcal{F} , a representation function $g : \mathcal{G} \rightarrow \mathbb{R}^n$ (e.g., GNN), and a loss function $\ell : \mathcal{Y} \times \mathcal{Y} \rightarrow \mathbb{R}$, the goal is to learn a predictor $f_c \in \mathcal{F}$ that minimizes the worst-case risk over \mathcal{E} .*

$$\min_{f_c \in \mathcal{F}} \max_{e \in \mathcal{E}} \mathbb{E}_{(G_v^e, y_v^e) \sim \mathbb{P}(G^e, Y^e)} \ell(f_c(g(G_v^e)), y_v^e) \quad (1)$$

We assume $\mathcal{E}_{train} \subsetneq \mathcal{E}$ is accessible during training and $\mathcal{E}_{test} = \mathcal{E} \setminus \mathcal{E}_{train}$ is an inaccessible and unknown test domain.

3.2 Assumptions

To tackle the problem mentioned above, we begin by establishing the following assumptions.

Assumption 1 (Multiple Latent Factors). *Given a subgraph G^e and the corresponding $\{(G_v^e, y_v^e)\}_{v=1}^{|\mathcal{V}^e|}$ from any domain $\forall e \in \mathcal{E}$. Given a representation function (e.g., GNN) $g : \mathcal{G} \rightarrow \mathbb{R}^n$, we assume that the representation of each node $\mathbf{z}_v^e = g(G_v^e)$ in G^e is generated from*

- a latent semantic factor $\mathbf{c} \in \mathcal{C}$, where $\mathcal{C} = \{\mathbf{c}_{y_v^e=0}, \mathbf{c}_{y_v^e=1}, \dots, \mathbf{c}_{y_v^e=C}\}$ denotes a semantic space and C is the number of label categories;
- a latent variation factor \mathbf{r}^e , where $\mathbf{r}^e = \{\mathbf{r}_a^e, \mathbf{r}_t^e\}$ is specific to the individual domain e . Herein, \mathbf{r}_a^e is the variation factor on attribute and \mathbf{r}_t^e is the variation factor on topology. The variation factor \mathbf{r}^e controls the change of domain e .

The above assumption indicates that for any two node representations, $\bar{v}_1 := \{\mathbf{z}_{v_1}^e, y_{v_1}^e\}$ sampled from G^e and $\bar{v}_2 := \{\mathbf{z}_{v_2}^{e'}, y_{v_2}^{e'}\}$ sampled from $G^{e'}$

- if $e = e'$ and $y_{v_1}^e = y_{v_2}^{e'}$, then \bar{v}_1 and \bar{v}_2 share the same \mathbf{c} and \mathbf{r}^e ;
- if $e = e'$ and $y_{v_1}^e \neq y_{v_2}^{e'}$, then \bar{v}_1 and \bar{v}_2 share the same \mathbf{r}^e , but different \mathbf{c} ;
- if $e \neq e'$ and $y_{v_1}^e = y_{v_2}^{e'}$, then \bar{v}_1 and \bar{v}_2 share the same \mathbf{c} , but different \mathbf{r}^e and $\mathbf{r}^{e'}$;
- if $e \neq e'$ and $y_{v_1}^e \neq y_{v_2}^{e'}$, then neither \mathbf{c} or \mathbf{r}^e and $\mathbf{r}^{e'}$ are the same for \bar{v}_1 and \bar{v}_2 .

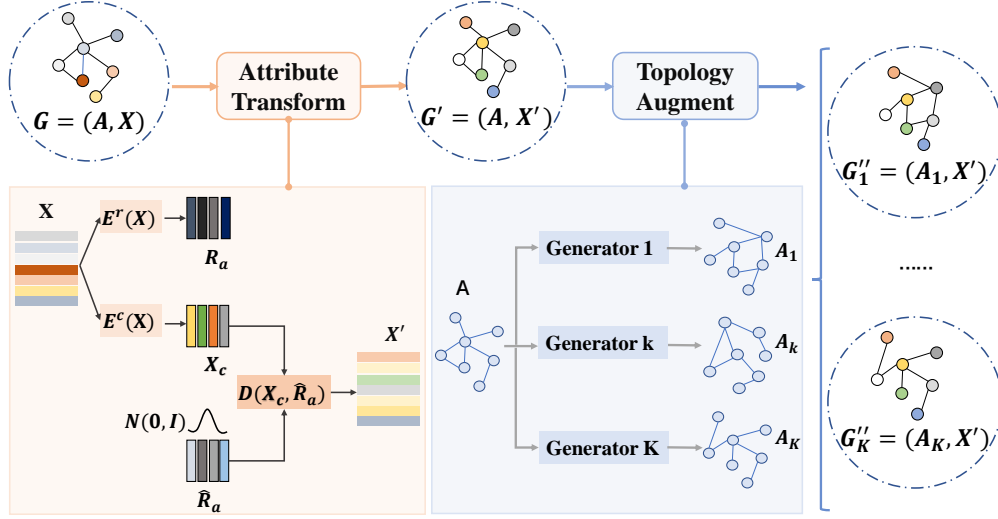


Figure 1: An overview of the GLIDER framework. First, GLIDER generates a G' that has the same topology, but a different attribute distribution with the input graph G . In this step, it learns a semantic feature encoder E^c , a variation feature encoder E^r , and a decoder D . Then it generates node attributes X' in new synthetic domains, wherein only the variation factor is replaced with a sampled one from $\mathcal{N}(0, \mathbf{I})$. Second, it learns generators that can generate K adjacent matrix with structure as differently as possible. Then we can generate K graphs $\{G''_k = (A_k, X')\}_{k=1}^K$ with different X and A compared with G .

Note that Assumption 1 is similar to [24, 25] and has been extensively employed in interpretability research [26, 27]. We extend the assumptions of existing works by introducing two latent factors to focus on graph data.

Assumption 2 (Invariance on Graphs). *We assume that inter-domain variation is solely characterized by domain shift in the marginal distributions $\mathbb{P}(Z^e)$, $\forall e \in \mathcal{E}$. We assume that $\mathbb{P}(Y^e | Z^e)$ is stable across domains. Given a domain transformation function \mathcal{T} , for any $\mathbf{z} \in \mathbb{R}^m$, $y \in \mathcal{Y}$, it holds that:*

$$\mathbb{P}(Y^e = y | Z^e = \mathbf{z}^e) = \mathbb{P}(Y^{e'} = y | Z^{e'} = \mathcal{T}(\mathbf{z}^e, e')), \forall e, e' \in \mathcal{E}, e \neq e' \quad (2)$$

Some recent works [7, 9] for node-level OOD generation on graphs problem have considered either topology variation [6, 7] or node attribute variation [8, 9] only. They do not take into account the variations that occur simultaneously. Based on Assumption 1, distribution shift across domains is determined by \mathbf{r}^e , $\forall e \in \mathcal{E}$ that includes variation factors for both node attribute \mathbf{r}_a^e and topology \mathbf{r}_t^e . Expanding on the insights from the existing literature [27], we emphasize that inter-domain variation is solely characterized by the domain shift on $\mathbb{P}(Z^e)$ due to \mathcal{T} .

4 Methodology

In this section, we will present GLIDER in detail. Fig. 1 shows an overview of GLIDER and its learning process. The algorithmic pseudocode of the whole framework is given at Algorithm 1.

4.1 Attribute Matrix Transformation

According to Assumption 1, an attribute vector \mathbf{x}^e of a node of a specific domain e is generated from a latent semantic factor \mathbf{x}_c , and a variation factor \mathbf{r}_a^e that is specific to the domain with A unchanged. We denote $R_a = [\mathbf{r}_a^{e_1}, \dots, \mathbf{r}_a^{e_{|\mathcal{E}|}}]$ as the variation matrix for transformation from G to G' .

We encode the attribute feature vector \mathbf{x} of each node in G into a latent semantic factor $\mathbf{x}_c \in \mathbb{R}^{d_c}$ and a latent variation factor $\mathbf{r}_a^e \in \mathbb{R}^{d_r}$. Our objective is to learn a domain-invariant semantic feature encoder E^c , domain-specific variation feature encoder E^r , and a decoder D to generate various attribute feature vectors for each node. To achieve this, we generate node attributes in new synthetic domains, wherein only the variation factor is replaced with a randomly sampled one. We draw some latent variation factor \hat{R}_a from the prior distribution $q(\hat{R}_a) \sim \mathcal{N}(0, \mathbf{I})$. These generated $\hat{\mathbf{r}}_a$ and \mathbf{x}_c are used to generate multiple attribute feature vectors preserving invariant information, i.e., $\mathbf{x}' = D(\mathbf{x}_c, \hat{\mathbf{r}}_a)$. In

the same way, we also encode the generated \mathbf{x}' into a latent semantic factor \mathbf{x}'_c and a latent variation factor \mathbf{r}'_a . Herein, \mathbf{x}_c and \mathbf{x}'_c should theoretically be equivalent. A new graph, $G' = (A, X')$, with the same topology as G but different attribute distribution of node, can be generated, where $X' = [\mathbf{x}'_1, \mathbf{x}'_2, \dots, \mathbf{x}'_{|\mathcal{V}|}]$. To accomplish the above objectives, we define the loss function of this process. The loss comprises a bidirectional reconstruction loss to guarantee that the encoders and decoder work inversely, and an adversarial loss to align the distribution of the translated and original feature matrix.

Bidirectional reconstruction loss. To learn mutually inverse pairs of encoder and decoder, we utilize objective functions that encourage reconstruction in both the matrix \rightarrow latent \rightarrow matrix and latent \rightarrow matrix \rightarrow latent directions.

- *Matrix reconstruction.* We use encoding and decoding to reconstruct the attribute feature matrix that was sampled from the data distribution. The objective function can be formulated as the following:

$$\mathcal{L}_{rec}^x = \mathbb{E}_{X \sim \mathbb{P}(X)} [\|D(X_c, R_a), X\|_1], \quad (3)$$

where $X_c = E^c(X)$ and $R_a = E^r(X)$.

- *Latent reconstruction.* Given a latent semantic factor and a variation factor sampled from the prior distribution $\mathcal{N}(0, \mathbf{I})$, we should attempt to reconstruct it after decoding and encoding.

$$\mathcal{L}_{rec}^c = \mathbb{E}_{X_c \sim \mathbb{P}(C), \hat{R}_a \sim q(\hat{R}_a)} [\|E^c(D(X_c, \hat{R}_a)) - X_c\|_1], \quad (4)$$

$$\mathcal{L}_{rec}^r = \mathbb{E}_{X_c \sim \mathbb{P}(C), \hat{R}_a \sim q(\hat{R}_a)} [\|E^r(D(X_c, \hat{R}_a)) - \hat{R}_a\|_1], \quad (5)$$

where $q(\hat{R}_a)$ is the prior $\mathcal{N}(0, \mathbf{I})$, $\mathbb{P}(C)$ is given by $X_c = E^c(X)$. The semantic feature reconstruction loss \mathcal{L}_{rec}^c has the effect of encouraging the translated matrix to preserve the semantic feature of the input matrix. The variation feature reconstruction loss \mathcal{L}_{rec}^r is capable of generating diverse outputs given diverse variation factors.

Adversarial loss. To guarantee the matrix generated by our model is indistinguishable from the real feature matrix in the target domain, we employ *maximizing mutual information* to match the distribution of the translated matrix to the real data. We employ a discriminator $\Psi: \mathcal{G} \rightarrow \mathbb{R}$, where $\Psi(D(X_c, \hat{R}_a))$ represents the probability scores of similarity between translated and real matrix. Negative samples X' for Ψ are generated by pairing the semantic latent factor with a latent variation factor sampled from the $\mathcal{N}(0, \mathbf{I})$. The objective is formulated as follows:

$$\mathcal{L}_{Di} = \mathbb{E}_{X' \sim \mathbb{P}(X')} [\log(1 - \Psi(X'))] + \mathbb{E}_{X \sim \mathbb{P}(X)} [\log \Psi(X)], \quad (6)$$

where $X' = D(X_c, \hat{R}_a)$. This approach effectively maximizes the mutual information between X' and X .

Total loss. We jointly train the encoders, decoder, and discriminators to optimize the final objective, which is a weighted sum of the adversarial loss and the bidirectional reconstruction loss terms.

$$\mathcal{L} = \mathcal{L}_{Di} + \lambda_x \mathcal{L}_{rec}^x + \lambda_c \mathcal{L}_{rec}^c + \lambda_s \mathcal{L}_{rec}^r, \quad (7)$$

where $\lambda_x, \lambda_c, \lambda_s$ are the weight coefficient of each part.

4.2 Topology Augmentation

Given a graph $G' = (A, X')$ generated from the original graphs G , we now demonstrate the generation of a sequence of graph $\{G''_k = (A_k, X'')\}_{k=1}^K$. In contrast to G' , each G''_k in the sequence maintains the node attribute X' and changes the topological structure from A to A_k . We define K graph generators $\{\hat{g}_{w_k}\}_{k=1}^K$. Herein, the goal of our framework is to learn generators $\{\hat{g}_{w_k}\}_{k=1}^K$ with parameters $\{w_1, \dots, w_K\}$, where $\hat{g}_{w_k}(G') = G''_k = (A_k, X')$. These generators are devoted to generating K graphs with the least possible similarity in their node topologies. For simplicity, we use G^k to represent the G''_k in this section.

To begin, we define the mean value of prediction losses for all nodes in a generated graph as $l_k = \frac{1}{|\mathcal{V}|} \sum_{v \in \mathcal{V}} \ell(f_c(g(G_v^k), y_v^k))$, where $G^k = \hat{g}_{w_k}(G')$ and G_v^k is corresponding ego-graph of node v in G^k . To enhance topological differences among graphs, we train generators by maximizing the variance of l_k across them:

$$\max_{w_1, \dots, w_K} \mathbb{V}(l_k) : (1 \leq k \leq K). \quad (8)$$

Inspired by [28], we use the data augmentation method of adding and subtracting edges to learn the generator \hat{g}_{w_k} . We define a Boolean matrix $\bar{R}_t^k = \{0, 1\}^{|\mathcal{V}| \times |\mathcal{V}|}$ ($k = 1, \dots, K$) and the supplement matrix of A as $\bar{A} = \mathbf{1}\mathbf{1}^T - I - A$, where I is an identity matrix and $\mathbf{1}$ is a vector of length $|\mathcal{V}|$ with each element is 1. Element in the matrix \bar{R}_t^k represents

whether the two nodes in the corresponding position are connected by an edge. Then a new topology matrix is obtained by $A_k = A + \bar{R}_t^k \circ (\bar{A} - A)$, where \circ denotes the element-wise product. However, \bar{R}_t^k is indifferentiable and the objective function is non-convex. To solve this dilemma, we introduce the policy gradient method to optimize the \hat{g}_{w_k} , which regards the generation of graphs as a decision process and edge operation as actions. We define a parameterized matrix set $\mathcal{B} = \{B_1, B_2, \dots, B_K\}$, where $B_k = \{\beta_{ij}^k\}$. Take the i -th node as an example, the probability of editing the edge between node i and node j for the i -th node in view k is $p(\sigma_{ij}^k) = \frac{\exp(\beta_{ij}^k)}{\sum_{j' \in \mathcal{V}} \exp(\beta_{ij'}^k)}$. Then we execute s actions $\{s_{ijt}^k\}_{t=1}^s$ from a multinomial distribution $\Omega(p(\sigma_{i1}^k), p(\sigma_{i2}^k), \dots, p(\sigma_{i|\mathcal{V}|}^k), \dots, p(\sigma_{|\mathcal{V}||\mathcal{V}|}^k))$, which determines the non-zero element in row i of \bar{R}_t^k . Moreover, we define the reward function Q as the inverse of the loss in Eq. (8). Herein, we utilize REINFORCE [29] algorithm to optimize the w_k with the gradient $\nabla_{w_k} \log p_{w_k}(A_k)Q$, where $w_k = B_k$ and $p_{w_k}(A_k) = \prod_{i=1}^{|\mathcal{V}|} \prod_{t=1}^s p(s_{ijt}^k)$.

4.3 Invariant Representation Learning

Once we complete the initial two steps, we produce K graphs G'' that display a different distribution of attributes and topology of nodes. Then we will extract the ego-graph G_v'' for each node v in G'' and generate a series of instances $\{(G_v'', y_v'')\}_{v \in \mathcal{V}''}$. For Problem 1, we utilize GNN as the representation function g , which learns the representation of each node by iteratively aggregating the neighbors' information of the center node in the ego-graph. Please note that in this context, G'' refers to a graph that has been sampled from various domains. To maintain consistency, we will continue to use e to represent a distinct domain in the following text.

We assume that when the variance of empirical risk across different environments is smaller, the model tends to make predictions with invariant characteristics, *i.e.*, when the objective $\min \mathbb{V}_e[R(e)]$ reaches the optimum. So we get the following objective:

$$\min \mathbb{V}_e[\ell(f_c(g(G_v^e)), y_v^e)] + \alpha \mathbb{E}_e[\ell(f_c(g(G_v^e)), y_v^e)] \quad (9)$$

where α is a weight coefficient.

5 Theoretical Analysis

Under Assumption 1 and Assumption 2, if we restrict the domain \mathcal{F} to the set of domain-invariant predictors, then Problem 1 is equivalent to the following constrained optimization problem:

$$\begin{aligned} P^* &\triangleq \min_{f_c \in \mathcal{F}} R(f_c) \triangleq \mathbb{E}_{\mathbb{P}(Z, Y)} \ell(f_c(\mathbf{z}), y) \\ \text{s.t. } &f_c(\mathbf{z}) = f_c(\mathcal{T}(\mathbf{z}, e)) \quad \text{a.e. } \mathbf{z} \sim \mathbb{P}(Z), \forall e \in \mathcal{E} \end{aligned} \quad (10)$$

where $\mathbf{z} = g(G_v^e)$ and $R(f_c)$ is the statistical risk of a predictor f_c . However, enforcing a hard invariance constraint on the class \mathcal{F} is not clear a priori. To render it more tractable, we introduce the following relaxation of Eq. (10):

$$\begin{aligned} P^*(\gamma) &\triangleq \min_{f_c \in \mathcal{F}} R(f_c) \\ \text{s.t. } &\mathcal{L}^e(f_c) \triangleq \mathbb{E}_{\mathbb{P}(Z)} h(f_c(\mathbf{z}), f_c(\mathcal{T}(\mathbf{z}, e))) \leq \gamma, \forall e \in \mathcal{E}, \end{aligned} \quad (11)$$

where $\gamma > 0$ is a fixed margin that regulates the difference between classifiers in various environments and $h: \mathcal{P}(\mathcal{Y}) \times \mathcal{P}(\mathcal{Y}) \rightarrow \mathbb{R}_{\geq 0}$ is a distance metric between different distributions. By relaxing the equality constraints in Eq. (10) to the inequality constraints in Eq. (11) and under appropriate conditions on ℓ and h , Eq. (11) can be characterized using the constrained PAC learning framework. This framework is capable of providing learnability guarantees on constrained statistical problems. Furthermore, when assuming that the perturbation function $P^*(\gamma)$ is L-Lipschitz continuous and γ is strictly greater than zero, we have that $|P^* - P^*(\gamma)| \leq L\gamma$, which means the discrepancy between the Eq. (10) and Eq. (11) is relatively small when a small value of γ is selected. Eq. (11) poses an infinite-dimensional constrained optimization problem over a functional space \mathcal{F} , rendering it intractable. Therefore, to address this challenge, we follow the standard convention by leveraging a finite-dimensional parameterization of \mathcal{F} . We can quantify the approximation power of such a parameterization using the following definition:

Definition 1 (ϵ -parameterization). Let $\mathcal{H} \subseteq \mathbb{R}^p$ be a finite-dimensional parameter space. For $\epsilon > 0$, a function $\varphi: \mathcal{H} \times \mathcal{Z} \rightarrow \mathcal{Y}$ is said to be an ϵ -parameterization of \mathcal{F} if it holds that for each $f_c \in \mathcal{F}$, there exists a parameter $\theta \in \mathcal{H}$ such that $\mathbb{E}_{\mathbb{P}(Z)} \|\varphi(\theta, \mathbf{z}) - f_c(\mathbf{z})\|_{\infty} \leq \epsilon$. Then, optimizing Eq. (10) becomes tractable when dealing with a

Algorithm 1 GLIDER.

1: **Input:** an input graph $G = (A, X)$ and labels \mathcal{Y} , initialized parameters θ of GNN, learning rates l_f, l_g , hyperparameter α , graph editors $\{w_k\}_{k=1}^K$.

2: **Repeat:**

3: $X' \leftarrow \text{GENERATE}(X)$

4: $\{G'_k\}_{k=1}^K \leftarrow \text{AUGMENTATION}(A, X')$

5: $\text{Loss } \mathcal{L} \leftarrow \text{compute using Eq. (9)}$

6: Update $\theta \leftarrow \theta - l_f \nabla_{\theta} \mathcal{L}(\theta)$

7: **Until** convergence

8:

9: **Procedure** $\text{GENERATE}(X)$

10: **Repeat:**

11: $(X_c, X_{r_a}) \leftarrow E^c(X), E^r(X)$

12: Sample $\hat{r}_a \sim \mathcal{N}(0, \mathbf{I})$

13: $X' = D(X_c, \hat{r}_a)$

14: Compute loss $\mathcal{L}_{rec}^x, \mathcal{L}_{rec}^c, \mathcal{L}_{rec}^r, \mathcal{L}_{Di}$, and \mathcal{L} in Eq. (3), Eq. (4), Eq. (5), Eq. (6) and Eq. (7)

15: **Until** convergence

16: **End procedure**

17:

18: **Procedure** $\text{AUGMENTATION}(G')$

19: **For** $t = 1, \dots, T$ **do**

20: Generated graphs $G^k = (A_k, X')$ from graph generator $\hat{g}_{w_k}, k = 1, \dots, K$

21: Compute loss $\mathcal{L}(w) = \mathbb{V}(l_k)$ in Eq. (8)

22: Update $w_k \leftarrow w_k + l_g \nabla_{w_k} \log p_{w_k}(A_k) \mathcal{L}(w)$

23: **End for**

24: **End procedure**

finite parametric space $\mathcal{U}_\epsilon := \{\varphi(\theta, \cdot) : \theta \in \mathcal{H}\} \subseteq \mathcal{F}$. To solve the above parameterization problem, we consider the following saddle-point problem:

$$D_\epsilon^*(\gamma) \triangleq \max_{\tau \in \mathcal{P}(\mathcal{E})} \min_{\theta \in \mathcal{H}} R(\theta) + \int_{\mathcal{E}} [\mathcal{L}^e(\theta) - \gamma] d\tau(e), \quad (12)$$

where $\mathcal{P}(\mathcal{E})$ denotes the space of normalized probability distributions over \mathcal{E} and $\tau \in \mathcal{P}(\mathcal{E})$ denotes the (semi-infinite) dual variable. Let $\gamma > 0$ and there exists a small universal constant t , the optimality gap between Eq. (11) and Eq. (12) can be explicitly bounded as follows:

$$P^*(\gamma) \leq D_\epsilon^*(\gamma) \leq P^*(\gamma) + \epsilon t(1 + \|\tau_{pert}^*\|_1), \quad (13)$$

where τ_{pert}^* is the optimal dual variable for a perturbed version of Eq. (11) in which the constraints are tightened to maintain a margin $\gamma - t\epsilon$. This reveals that the difference between $P^*(\gamma)$ and $D_\epsilon^*(\gamma)$ is small when employing the ϵ -parameterization on \mathcal{F} . Nevertheless, we do not have access to $\mathcal{E} \setminus \mathcal{E}_{train}$. In practice, it is ubiquitous to solve optimization problems such as Eq. (12) over a finite sample of N data points. Thus, given $\{(\mathbf{z}_{v_i}, y_{v_i})\}_{i=1}^N$ drawn *i.i.d* from $\mathbb{P}(Z, Y)$, we consider the empirical counterpart of Eq. (12):

$$\begin{aligned} D_{\epsilon, N, \mathcal{E}_{train}}^*(\gamma) &\triangleq \max_{\tau(e) \geq 0, e \in \mathcal{E}_{train}} \min_{\theta \in \mathcal{H}} \Gamma(\theta, \tau) \\ &\triangleq \hat{R}(\theta) + \frac{1}{|\mathcal{E}_{train}|} \sum_{e \in \mathcal{E}_{train}} [\hat{\mathcal{L}}^e(\theta) - \gamma] \tau(e), \end{aligned} \quad (14)$$

where $\hat{R}(\theta) := \frac{1}{N} \sum_{i=1}^N l(\varphi(\theta, \mathbf{z}_{v_i}), y_{v_i})$ and $\hat{\mathcal{L}}^e(\theta) := \frac{1}{N} \sum_{i=1}^N d(\varphi(\theta, \mathbf{z}_{v_i}), \varphi(\theta, \mathbf{z}_{v_i}^e))$. $\Gamma(\theta, \tau)$ is the empirical Lagrangian. We can explicitly bound the duality gap between the solution to Eq. (14) and the original Problem 1 in the following way.

Theorem 1 (Data-dependent duality gap). *Given $\epsilon > 0$ and let φ be an ϵ -parameterization of \mathcal{F} . Under mild regularity assumptions on l and h and assuming that \mathcal{U} has finite VC-dimension, with probability $1 - \rho$ over the N samples representations from $\mathbb{P}(Z, Y)$, we have that*

$$|P^* - D_{\epsilon, N, \mathcal{E}_{train}}^*(\gamma)| \leq L\gamma + \epsilon t(1 + \|\tau_{pert}^*\|_1) + \mathcal{O}(\sqrt{\log(N)/N}), \quad (15)$$

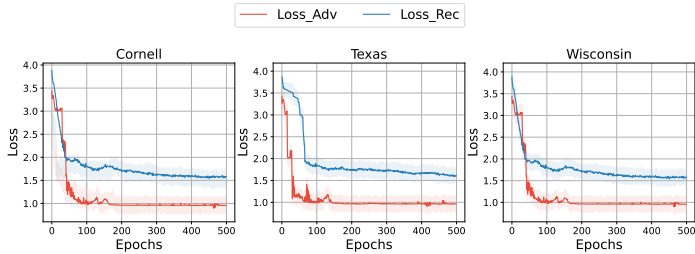


Figure 2: Loss curve of training discriminator where Loss_Adv represents the adversarial loss and Loss_Rec represents the reconstruction loss.

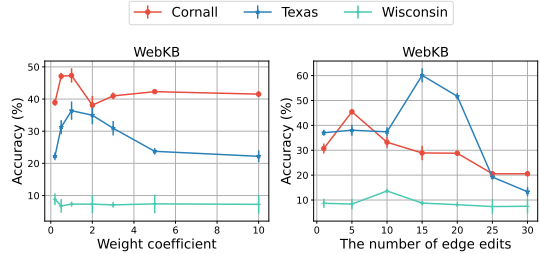


Figure 3: Sensitivity of GLIDER w.r.t the weight coefficient in Eq. (9) and the number of edits for each node by the edge.

Table 1: Test accuracy (%) comparison on WEBKB.

Methods	Cornell	Texas	Wisconsin	Avg
EERM	19.2 ± 1.3	31.1 ± 2.1	7.7 ± 1.7	19.4
ERM	12.8 ± 2.0	42.8 ± 6.9	13.5 ± 1.2	23.0
IRM	15.3 ± 0.7	11.9 ± 4.1	13.4 ± 0.9	13.5
DANN	15.8 ± 2.2	18.2 ± 3.5	14.1 ± 1.1	16.1
VREx	15.3 ± 1.0	15.8 ± 2.9	14.0 ± 1.7	15.0
SRGNN	15.8 ± 0.6	14.3 ± 2.8	8.7 ± 2.5	12.9
Mixup	25.7 ± 2.1	20.6 ± 1.0	13.8 ± 2.8	20.0
GroupDRO	15.8 ± 1.3	14.3 ± 0.7	13.0 ± 1.5	14.4
GLIDER-C	25.1 ± 4.8	30.6 ± 5.4	8.8 ± 1.0	21.5
GLIDER-A	41.8 ± 0.7	32.8 ± 0.4	8.7 ± 0.0	27.8
GLIDER	44.4 ± 0.9	46.0 ± 0.1	14.1 ± 1.6	34.8

where L is the Lipschitz constant of $P^*(\gamma)$.

Assuming that both Assumption 1 and 2 hold, the Problem 1 is closely approximated by the duality gap in Eq. (14) when 1) the γ is small, 2) \mathcal{U} is a close approximation of \mathcal{F} , and 3) there are enough samples being observed. We provide the proof of Theorem 1 in Appendix C.1.

6 Experiment Settings

Datasets. In our experiments, we adopt four real network datasets, TWITCH-EXPLICIT [30], FACEBOOK-100 [31], WEBKB [32] and DBLP [33]. Each dataset contains a different number of graphs and more details are shown in Appendix B.1.

Baselines. We compare our model GLIDER with standard empirical risk minimization (ERM), 3 graph-specific methods (EERM [23], SRGNN [34], and Mixup [35]), and other 3 OOD algorithms (IRM [36], DANN [37], and VREx [19]). More baselines details are presented in Appendix B.2.

Settings for Domain Generalization. We follow the principle of multiple graph training. In the TWITCH dataset, we adopt a sequential approach where one out of the seven graphs is selected for testing, while the remaining six graphs are utilized for training and validation. In FACEBOOK-100, following [23], we designate Penn, Brown, and Texas for testing, employing three distinct combinations from the remaining graphs for training, Hopkins + Caltech + Amherst, Bingham + Duke + Princeton and WashU + Brandeis+ Carnegie. For WEBKB and DBLP, we alternate the utilization of three graphs of the dataset as testing domains. We utilize GCN as the backbone model and evaluate its performance using test accuracy and F1 score on four datasets. In addition, the hyperparameter settings are provided in Appendix. B.3.

7 Experimental Results

Visualization and Analysis. We conducted experiments to evaluate the performance of GLIDER on node classification tasks. The results are reported in Table 1 - Table 7. Due to space constraints, the results of accuracy on TWITCH and the F1 score on TWITCH and FB-100 are shown in Appendix C.2. The training process is repeated 5 times, and the resulting average is considered the final result. As observed from the result, we have the following findings.

Table 2: Test accuracy (%) comparison on DBLP.

Methods	D1	D2	D3	Avg
EERM	43.3 ± 3.7	53.0 ± 3.0	49.6 ± 3.1	48.6
ERM	38.3 ± 2.4	51.3 ± 0.2	50.0 ± 1.5	46.5
IRM	35.6 ± 0.7	40.8 ± 2.1	43.4 ± 0.2	39.9
DANN	39.1 ± 1.2	42.8 ± 1.4	43.6 ± 2.1	41.8
VREx	43.5 ± 0.4	46.2 ± 2.4	45.9 ± 0.2	45.2
SRGNN	44.7 ± 0.8	47.2 ± 1.9	47.0 ± 2.6	46.3
Mixup	45.9 ± 1.7	47.1 ± 2.0	48.3 ± 0.9	47.1
GroupDRO	46.2 ± 1.5	49.3 ± 1.7	48.4 ± 0.3	48.0
GLIDER-C	50.3 ± 1.8	50.9 ± 0.2	47.4 ± 2.1	49.5
GLIDER-A	50.2 ± 0.3	52.8 ± 0.1	49.5 ± 1.0	50.8
GLIDER	51.9 ± 1.0	53.2 ± 2.6	50.1 ± 1.1	51.8

Table 3: Test accuracy (%) on FB-100 where we compare different configurations of training graphs.

Methods	Hopkins + Caltech + Amherst				Bingham + Duke + Princeton				WashU + Brandeis+ Carnegie			
	Penn	Brown	Texas	Avg	Penn	Brown	Texas	Avg	Penn	Brown	Texas	Avg
EERM	50.9 ± 1.4	55.4 ± 4.1	53.8 ± 4.6	53.4	50.7 ± 2.2	48.2 ± 4.2	50.6 ± 5.4	49.8	50.5 ± 1.2	47.3 ± 1.9	51.2 ± 4.1	49.7
ERM	50.1 ± 1.5	54.7 ± 4.7	55.1 ± 2.4	53.3	47.3 ± 0.5	47.4 ± 4.4	50.5 ± 4.6	48.4	49.8 ± 0.6	43.9 ± 4.5	47.6 ± 4.1	47.1
IRM	45.3 ± 0.2	42.1 ± 1.2	39.4 ± 1.1	42.3	46.7 ± 0.1	43.6 ± 2.2	40.3 ± 1.1	43.5	47.7 ± 0.4	44.8 ± 1.0	42.3 ± 2.8	45.0
DANN	42.1 ± 0.2	43.4 ± 2.1	46.6 ± 3.4	44.1	41.7 ± 0.4	42.8 ± 1.1	45.4 ± 0.8	43.3	43.6 ± 1.1	44.8 ± 2.2	45.5 ± 1.3	44.6
VREx	41.5 ± 2.4	50.7 ± 2.1	47.9 ± 2.1	46.7	42.0 ± 0.7	50.6 ± 1.7	46.9 ± 1.9	46.5	45.6 ± 1.2	51.2 ± 2.1	45.9 ± 2.8	47.6
SRGNN	40.3 ± 1.7	41.1 ± 0.8	46.4 ± 1.0	42.6	39.9 ± 0.9	40.3 ± 1.5	44.9 ± 2.1	41.7	43.5 ± 2.1	42.3 ± 0.9	43.9 ± 1.1	43.3
Mixup	50.6 ± 2.1	45.4 ± 3.1	48.9 ± 3.1	48.3	50.5 ± 2.0	46.1 ± 0.8	46.9 ± 1.5	47.9	50.0 ± 1.9	45.1 ± 1.6	45.9 ± 2.3	47.0
GroupDRO	48.2 ± 2.4	49.7 ± 1.0	50.0 ± 1.3	49.3	47.1 ± 1.3	48.8 ± 0.9	49.9 ± 1.6	48.6	46.8 ± 0.1	47.5 ± 1.9	48.2 ± 2.1	47.5
GLIDER-C	49.9 ± 0.6	55.8 ± 2.8	55.2 ± 3.2	53.7	49.9 ± 1.1	54.4 ± 2.2	56.3 ± 0.0	53.6	50.1 ± 0.9	56.8 ± 2.2	56.3 ± 1.7	54.5
GLIDER-A	49.8 ± 0.7	56.0 ± 2.1	55.2 ± 3.1	53.7	50.9 ± 0.1	56.9 ± 0.0	56.4 ± 0.0	54.7	50.0 ± 0.7	51.8 ± 1.7	51.5 ± 2.5	51.1
GLIDER	50.9 ± 0.8	58.0 ± 0.3	56.3 ± 0.0	55.1	50.8 ± 0.0	54.4 ± 3.6	53.9 ± 3.2	53.1	50.5 ± 0.7	56.9 ± 2.3	56.3 ± 0.0	54.6

Firstly, GLIDER outperforms current state-of-the-art methods. EERM ranks second only to our model for multi-graph generalization in Table 2, Table 3, and Table 6. In contrast, EERM does not achieve the second-best performance in Table 1. This is because WEBKB is very sparse, and the EERM generates domains by randomly adding and subtracting edges. This introduces significant changes to the graph, thereby increasing the difficulty of invariant learning. We generate diverse domains through attribute matrix transition and topology augment, aiming to maximize graph variations while preserving semantic information. The augmentation applied in both attribute and topology structures in GLIDER is deemed more realistic.

Secondly, the compared approaches show varied performances amidst distinct distribution shifts. Traditional invariant learning algorithms such as IRM and VREx exhibit lower performance compared to graph data augmentation methods. This discrepancy arises from the strong dependence of invariant learning on the environment. The former predominantly relies on real multi-graph inputs to extract invariant information, whereas the latter can construct environments with maximum variability to enhance model generalization. Compared with the general OOD method, the graph-based OOD method has better performance, which shows that graph-based OOD is more effective for classifying tasks on graphs.

In addition, we evaluate the impact of various GNN backbones on the framework. We separately utilize GAT, SAGE, and GPR as the GNN models on WEBKB. The accuracy and F1 score results above demonstrate that EERM and ERM outperform other baseline methods. Therefore, we solely compare the performance of EERM and ERM with GLIDER using different backbones on WEBKB and report the results in Fig. 4. We observed that our model significantly outperforms EERM and ERM, with a maximum improvement of 13.0% in accuracy. This phenomenon demonstrates the universality and robustness of our model.

We also illustrate how the loss of the first module, attribute matrix transformation, changes as the epoch increases in Fig. 2. The loss of the first stage contains the adversarial loss and the reconstruction loss, both of which converge to stop the training process. In conclusion, GLIDER maintains the superiority of training graphs having distribution shifts, thus affirming the effectiveness of our model in addressing node-level OOD generation.

Ablation Study. To investigate the contribution of each module in GLIDER, we individually remove two key modules, namely attribute matrix transformation and topology augmentation. (1) We remain the semantic feature reconstruction \mathcal{L}_{rec}^c and remove the other part, which we define as GLIDER-C. (2) We generate multiple graphs with attribute distribution shifts while keeping the topology structures identical. We refer to this variant as GLIDER-A.

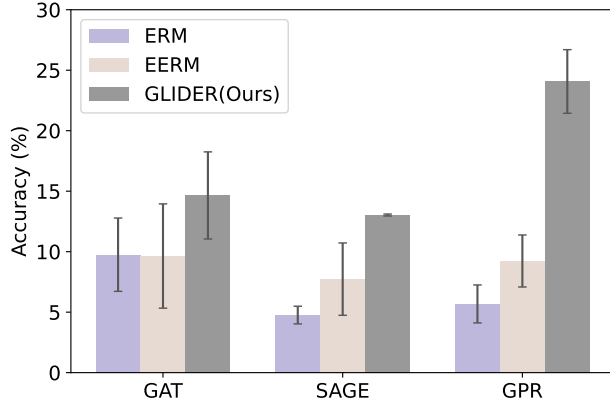


Figure 4: The accuracy of GLIDER (Ours) and another two baseline methods using different GNN backbones on WEBKB.

The results are shown in Table 1 - Table 7. Due to limited space, some results are available in Appendix C.2. We can see that: (1) the performance of GLIDER-C is slightly inferior to GLIDER on all datasets. Compared with EERM which does not perform the transformation on the attribute distribution, the performance of GLIDER-C is still elevated. This phenomenon shows that the reconstruction of domain-specific variation factor also plays a prominent role, and (2) Compared with EERM, which does not generate multiple environments using topology structure augmentation, GLIDER-A exhibits superior performance. This indicates that minimizing the prediction variance of multiple input graphs with the largest possible difference in topology is effective for addressing the OOD problem.

Sensitivity Analysis. We evaluated the sensitivity of our model regarding the α and s parameters on WEBKB and show the result in Fig. 3. α is the weight for combination, while s is the number of editing per node by edge.

Intuitively, we observe that as the value of α changes, the accuracy on all three graphs tends to stabilize when α is greater than 4. Therefore, GLIDER is robust to parameters α . The variation of accuracy values in the three graphs tends to stabilize with the increase of s , and we determine the value of s that yields the highest accuracy as the optimal model parameter. Specifically, the optimal s values differ for the three graphs. The parameter s exhibits varying degrees of influence on different graphs, likely due to the discrepancy in network density among the graphs.

8 Conclusion

In this paper, we propose an effective framework GLIDER for node-level OOD generation on graphs. We diversify the variation by modeling the potential seen or unseen variations of attribute distribution and topology of nodes and then minimize the semantic gap for each class among these variations. First, GLIDER generates multiple domains by attribute matrix transition and topology augmentation, and the distributions of node attributes and topology vary across domains. Then, we train a domain-invariant classifier by minimizing the empirical risk from multiple domains to learn the invariant information of nodes. Finally, we construct abundant experiments to evaluate the effectiveness of our framework in the node classification task, and the experimental results show that our method is superior to some baseline methods.

Acknowledgments

References

- [1] Krikamol Muandet, David Balduzzi, and Bernhard Schölkopf. Domain generalization via invariant feature representation. In *International Conference on Machine Learning*, pages 10–18. PMLR, 2013.
- [2] Alexander Robey, George J Pappas, and Hamed Hassani. Model-based domain generalization. *Advances in Neural Information Processing Systems*, 34:20210–20229, 2021.
- [3] Weihua Hu, Matthias Fey, Marinka Zitnik, Yuxiao Dong, Hongyu Ren, Bowen Liu, Michele Catasta, and Jure Leskovec. Open graph benchmark: Datasets for machine learning on graphs. *Advances in neural information processing systems*, 33:22118–22133, 2020.

- [4] Shuo Yang, Zhiqiang Zhang, Jun Zhou, Yang Wang, Wang Sun, Xingyu Zhong, Yanming Fang, Quan Yu, and Yuan Qi. Financial risk analysis for smes with graph-based supply chain mining. In *Proceedings of the Twenty-Ninth International Conference on International Joint Conferences on Artificial Intelligence*, pages 4661–4667, 2021.
- [5] Chirag Agarwal, Himabindu Lakkaraju, and Marinka Zitnik. Towards a unified framework for fair and stable graph representation learning. In *Uncertainty in Artificial Intelligence*, pages 2114–2124. PMLR, 2021.
- [6] Hyeonjin Park, Seunghun Lee, Sihyeon Kim, Jinyoung Park, Jisu Jeong, Kyung-Min Kim, Jung-Woo Ha, and Hyunwoo J Kim. Metropolis-hastings data augmentation for graph neural networks. *Advances in Neural Information Processing Systems*, 34:19010–19020, 2021.
- [7] Lirong Wu, Haitao Lin, Yufei Huang, and Stan Z Li. Knowledge distillation improves graph structure augmentation for graph neural networks. *Advances in Neural Information Processing Systems*, 35:11815–11827, 2022.
- [8] Wenzheng Feng, Jie Zhang, Yuxiao Dong, Yu Han, Huanbo Luan, Qian Xu, Qiang Yang, Evgeny Kharlamov, and Jie Tang. Graph random neural networks for semi-supervised learning on graphs. *Advances in neural information processing systems*, 33:22092–22103, 2020.
- [9] Kezhi Kong, Guohao Li, Mucong Ding, Zuxuan Wu, Chen Zhu, Bernard Ghanem, Gavin Taylor, and Tom Goldstein. Robust optimization as data augmentation for large-scale graphs. In *Proceedings of the IEEE/CVF Conference on Computer Vision and Pattern Recognition*, pages 60–69, 2022.
- [10] Yuning You, Tianlong Chen, Yongduo Sui, Ting Chen, Zhangyang Wang, and Yang Shen. Graph contrastive learning with augmentations. *Advances in neural information processing systems*, 33:5812–5823, 2020.
- [11] Yongduo Sui, Xiang Wang, Jiancan Wu, An Zhang, and Xiangnan He. Adversarial causal augmentation for graph covariate shift. *arXiv preprint arXiv:2211.02843*, 2022.
- [12] Hyunjik Kim and Andriy Mnih. Disentangling by factorising. In *International Conference on Machine Learning*, pages 2649–2658. PMLR, 2018.
- [13] Andrea Dittadi, Frederik Träuble, Francesco Locatello, Manuel Wüthrich, Vaibhav Agrawal, Ole Winther, Stefan Bauer, and Bernhard Schölkopf. On the transfer of disentangled representations in realistic settings. *arXiv preprint arXiv:2010.14407*, 2020.
- [14] Mengyue Yang, Furui Liu, Zhitang Chen, Xinwei Shen, Jianye Hao, and Jun Wang. Causalvae: Disentangled representation learning via neural structural causal models. In *Proceedings of the IEEE/CVF conference on computer vision and pattern recognition*, pages 9593–9602, 2021.
- [15] Yongduo Sui, Xiang Wang, Jiancan Wu, Min Lin, Xiangnan He, and Tat-Seng Chua. Causal attention for interpretable and generalizable graph classification. In *Proceedings of the 28th ACM SIGKDD Conference on Knowledge Discovery and Data Mining*, pages 1696–1705, 2022.
- [16] Vikas Garg, Adam Tauman Kalai, Katrina Ligett, and Steven Wu. Learn to expect the unexpected: Probably approximately correct domain generalization. In *International Conference on Artificial Intelligence and Statistics*, pages 3574–3582. PMLR, 2021.
- [17] Kaiyang Zhou, Ziwei Liu, Yu Qiao, Tao Xiang, and Chen Change Loy. Domain generalization: A survey. *IEEE Transactions on Pattern Analysis and Machine Intelligence*, 2022.
- [18] Juan L Gamella and Christina Heinze-Deml. Active invariant causal prediction: Experiment selection through stability. *Advances in Neural Information Processing Systems*, 33:15464–15475, 2020.
- [19] David Krueger, Ethan Caballero, Joern-Henrik Jacobsen, Amy Zhang, Jonathan Binas, Dinghuai Zhang, Remi Le Priol, and Aaron Courville. Out-of-distribution generalization via risk extrapolation (rex). In *International Conference on Machine Learning*, pages 5815–5826. PMLR, 2021.
- [20] Donglin Xia, Xiao Wang, Nian Liu, and Chuan Shi. Learning invariant representations of graph neural networks via cluster generalization. *Advances in Neural Information Processing Systems*, 36, 2024.
- [21] Xingxuan Zhang, Peng Cui, Renzhe Xu, Linjun Zhou, Yue He, and Zheyang Shen. Deep stable learning for out-of-distribution generalization. In *Proceedings of the IEEE/CVF Conference on Computer Vision and Pattern Recognition*, pages 5372–5382, 2021.
- [22] Jiashuo Liu, Zheyang Shen, Peng Cui, Linjun Zhou, Kun Kuang, Bo Li, and Yishi Lin. Stable adversarial learning under distributional shifts. In *Proceedings of the AAAI Conference on Artificial Intelligence*, volume 35, pages 8662–8670, 2021.
- [23] Qitian Wu, Hengrui Zhang, Junchi Yan, and David Wipf. Handling distribution shifts on graphs: An invariance perspective. *arXiv preprint arXiv:2202.02466*, 2022.
- [24] Ming-Yu Liu, Thomas Breuel, and Jan Kautz. Unsupervised image-to-image translation networks. *Advances in neural information processing systems*, 30, 2017.

- [25] Xun Huang, Ming-Yu Liu, Serge Belongie, and Jan Kautz. Multimodal unsupervised image-to-image translation. In *Proceedings of the European conference on computer vision (ECCV)*, pages 172–189, 2018.
- [26] Chang Liu, Xinwei Sun, Jindong Wang, Haoyue Tang, Tao Li, Tao Qin, Wei Chen, and Tie-Yan Liu. Learning causal semantic representation for out-of-distribution prediction. *Advances in Neural Information Processing Systems*, 34:6155–6170, 2021.
- [27] Hanlin Zhang, Yi-Fan Zhang, Weiyang Liu, Adrian Weller, Bernhard Schölkopf, and Eric P Xing. Towards principled disentanglement for domain generalization. In *Proceedings of the IEEE/CVF Conference on Computer Vision and Pattern Recognition*, pages 8024–8034, 2022.
- [28] Wei Jin, Yao Ma, Xiaorui Liu, Xianfeng Tang, Suhang Wang, and Jiliang Tang. Graph structure learning for robust graph neural networks. In *Proceedings of the 26th ACM SIGKDD international conference on knowledge discovery & data mining*, pages 66–74, 2020.
- [29] Junzi Zhang, Jongho Kim, Brendan O’Donoghue, and Stephen Boyd. Sample efficient reinforcement learning with reinforce. In *Proceedings of the AAAI conference on artificial intelligence*, volume 35, pages 10887–10895, 2021.
- [30] Benedek Rozemberczki, Carl Allen, and Rik Sarkar. Multi-scale attributed node embedding. *Journal of Complex Networks*, 9(2):cnab014, 2021.
- [31] Amanda L Traud, Peter J Mucha, and Mason A Porter. Social structure of facebook networks. *Physica A: Statistical Mechanics and its Applications*, 391(16):4165–4180, 2012.
- [32] Hongbin Pei, Bingzhe Wei, Kevin Chen-Chuan Chang, Yu Lei, and Bo Yang. Geom-gcn: Geometric graph convolutional networks. *arXiv preprint arXiv:2002.05287*, 2020.
- [33] Aleksandar Bojchevski and Stephan Günnemann. Deep gaussian embedding of graphs: Unsupervised inductive learning via ranking. *arXiv preprint arXiv:1707.03815*, 2017.
- [34] Qi Zhu, Natalia Ponomareva, Jiawei Han, and Bryan Perozzi. Shift-robust gnns: Overcoming the limitations of localized graph training data. *Advances in Neural Information Processing Systems*, 34:27965–27977, 2021.
- [35] Hongyi Zhang, Moustapha Cisse, Yann N Dauphin, and David Lopez-Paz. mixup: Beyond empirical risk minimization. *arXiv preprint arXiv:1710.09412*, 2017.
- [36] Martin Arjovsky, Léon Bottou, Ishaan Gulrajani, and David Lopez-Paz. Invariant risk minimization. *arXiv preprint arXiv:1907.02893*, 2019.
- [37] Yaroslav Ganin, Evgeniya Ustinova, Hana Ajakan, Pascal Germain, Hugo Larochelle, François Laviolette, Mario Marchand, and Victor Lempitsky. Domain-adversarial training of neural networks. *The journal of machine learning research*, 17(1):2096–2030, 2016.
- [38] Shiori Sagawa, Pang Wei Koh, Tatsunori B Hashimoto, and Percy Liang. Distributionally robust neural networks for group shifts: On the importance of regularization for worst-case generalization. *arXiv preprint arXiv:1911.08731*, 2019.

A Appendix

A.1 Notations

In this paper, vectors are denoted by lowercase boldface letters, *e.g.*, \mathbf{x} . Scalars are denoted by lowercase italic letters, *e.g.*, α and λ . Matrices are denoted by capital italic letters, *e.g.*, A . Sets are denoted by uppercase calligraphic letters, *e.g.*, \mathcal{E} . All notations used in this paper are listed in Table 4.

Table 4: Important notations and their description.

Notation	Description
G	An input graph
A	The adjacent matrix of a graph G
X	The attribute feature matrix of a graph G
G^e	A graph sampled from domain e
A^e	The adjacent matrix of a graph G^e
X^e	The attribute feature matrix of a graph G^e
\mathcal{V}	The node set of a graph G
$ \mathcal{V} $	The node number of a graph G
\mathbf{y}	The label of a graph G
\mathcal{G}	An input graph space
\mathcal{E}	The set of domain e
G_v^e	The ego-graph of node v in G^e
y_v^e	The label of node v in G^e
A_v^e	The adjacent matrix of G_v^e
X_v^e	The attribute feature matrix of G_v^e
f_c	A downstream classifier
\mathbf{c}	A latent semantic factor
\mathbf{r}^e	A latent variation factor from domain e
$\hat{\mathbf{r}}_a$	The variation factor of attributes draw from a prior distribution
\mathbf{r}_a^e	The variation factor on node attributes from domain e
G'	A graph where the attribute distribution of each node is shifted from the input graph G
G''	A graph where the attribute distribution and topology of each node are both shifted from the input graph
A'	A newly generated adjacency matrix
X'	A generated attribute matrix with distribution shifts
X_c	The latent semantic factor on the attribute of a graph
R_a	The latent variation factor on the attribute of a graph
E^c	A semantic encoder
E^r	A variation encoder
D	A decoder
Ψ	A discriminator
l_g, l_f	The learning rates
$\lambda_x, \lambda_c, \lambda_x, \alpha$	Weight coefficient for different loss
T	The number of iterations in topology augmentation
s	The number of edge editing actions for each node

B Datasets And Experimental Details

B.1 Dataset

The statistical characteristics of these networks are shown in Table 5.

Table 5: Key Characteristics of Datasets

Dataset	# Nodes	# Edges	# Class	#Feat	# Domain
TWITCH-EXPLICIT	20945	153,138	2	3170	7
FACEBOOK-100	131,924	1,590,655	2	12412	12
WEBKB	617	1138	5	1703	3
DBLP	17,716	105,734	4	1639	3

- TWITCH-EXPLICIT [30]. It is a gamer network that includes seven networks: DE, ENGB, ES, FR, PTBR, RU, and TW. Each network represents a particular game region. The aforementioned networks have comparable sizes but vary in terms of densities and maximum node degrees.
- FACEBOOK-100 [31]. This dataset comprises 100 snapshots of the *Facebook* friendship network, dating back to 2005. Each node represents a user from a particular American university, and the edges indicate the friendships between these users. We use twelve networks in our experiments: John Hopkins, Caltech, Amherst, Bingham, Duke, Princeton, WashU, Brandeis, Carnegie, Penn, Brown, and Texas.
- WEBKB [32]. It is a web page network dataset. The nodes in the network represent web pages, and the edges symbolize hyperlinks connecting these web pages. Additionally, the node features are represented using the bag-of-words representation of the web pages. The task is to classify the nodes into one of five categories: student, project, course, staff, and faculty. We split WEBKB into three networks (Cornell, Texas, and Wisconsin) according to the domain university.
- DBLP [33]. It is a citation network. Nodes represent publications and edges represent citation links between these publications. The task involves classifying publication types into 4 distinct classes. We generate three splits based on a domain selection (D1, D2, D3). The Domain is defined by the selected-word-count of a publication.

B.2 Compared Methods

- EERM [23] generates environments with diverse topologies and then minimizes the variances and mean values of predicted loss across different environments.
- IRM [36] aims to discover a latent invariant representation that remains consistent across all environments. This is achieved by penalizing feature distributions that exhibit varying optimal linear classifiers for each environment.
- DANN [37] learns to identify features that are indistinguishable between the training (source) and test (target) domains through adversarial training.
- VREx [19] solves the OOD problem by minimizing the variance of training risks based on the Risk Extrapolation (REx) model.
- SRGNN [34] is devoted to solving the distributional shift problem by converting biased data sets to unbiased data distribution. This is achieved using a central moment discrepancy regularizer and the kernel mean matching technique.
- Mixup [35] improves model generation capacity by constructing novel training examples drawn from raw data, thereby expanding the training distribution.
- GroupDRO [38] minimizes the worst-case training loss in all environments by increasing regularization on DRO groups.

B.3 Hyperparameter Tuning

The first module, attribute matrix transformation, include four hyperparameters: λ_x , λ_c , and λ_s . They are all weight coefficients of different parts in Eq. (7).

The parameters of the second module, topology augmentation, include four hyperparameters: α which denotes the weight coefficient of different parts in Eq. (9), K which denotes the number of generated adjacency matrices, T which denotes the number of iterations, and s which denotes the number of edge editing for each node.

We set $\alpha \in \{0.2, 0.5, 1.0, 2.0, 3.0, 5.0, 10.0\}$, $K \in \{1, 2, 3\}$, the learning rate $l_g, l_f \in \{0.0001, 0.0002, 0.001, 0.005, 0.01\}$, $T \in \{1, 5\}$, $s \in \{1, 5, 10, 15, 20, 25, 30\}$, weight coefficient $\lambda, \lambda_c, \lambda_s$ and λ_x are all in the range $[0, 1]$.

C Proofs

C.1 Sketch Proof of Theorem 1

The Theorem 1. Given $\epsilon > 0$ and let φ be an ϵ -parameterization of \mathcal{F} . Let l and d are under $[0, H]$ and both non-negative, convex. while assume that $d(\mathbb{P}, \mathbb{T}) = 0$ if and only if $\mathbb{P} = \mathbb{T}$. Then assuming that \mathcal{U} has finite VC-dimension with probability $1 - \rho$ over the N samples from \mathbb{P} that

$$|P^* - D_{\epsilon, N, \mathcal{E}_{train}}^*(\gamma)| \leq L\gamma + \epsilon t(1 + \|\tau_{pert}^*\|_1) + \mathcal{O}(\sqrt{\log(N)/N}), \quad (16)$$

Proof. First, let us assume $p^*(\gamma)$ is L-Lipschitz continuous in γ , when $d(\mathbb{P}, \mathbb{T}) = 0$ if and only if $\mathbb{P} = \mathbb{T}$ and $P^* = P^*(0)$, it follows that

$$\begin{aligned} |P^* - P^*(\gamma)| &= |P^*(0) - P^*(\gamma)| \\ &\leq L|0 - \gamma| \\ &= L\gamma \end{aligned} \quad (17)$$

Second, given $\gamma > 0$ and l and d are under $[0, H]$ and both non-negative, convex, we obtain that

$$P^*(\gamma) \leq D_\epsilon^*(\gamma) \leq P^*(\gamma) + \epsilon t(1 + \|\tau_{pert}^*\|_1) \cdot \max\{L_l, L_d\} \quad (18)$$

where τ_{pert}^* is the optimal dual variable for a perturbed version of Eq. (11) in which the constraints are tightened to hold with margin $\gamma - \epsilon \cdot \max\{L_l, L_d\}$. Then we get that

$$P^*(\gamma) - D_\epsilon^*(\gamma) \leq \epsilon t(1 + \|\tau_{pert}^*\|_1) \cdot \max\{L_l, L_d\} \quad (19)$$

Next, assuming that l and d are non-negative and bounded in $[-H, H]$ and \mathcal{U} has finite VC-dimension with probability $1 - \rho$ over the N samples from \mathbb{P} that

$$|D_\epsilon^* - D_{\epsilon, N, \mathcal{E}_{train}}^*(\gamma)| \leq 2H \sqrt{\frac{1}{N} \left[1 + \log\left(\frac{4(2N)^{d_{VC}}}{\rho}\right) \right]}, \quad (20)$$

By combining Eq. (17), Eq. (19) and Eq. (20), we obtain that

$$\begin{aligned} |P^* - D_{\epsilon, N, \mathcal{E}_{train}}^*(\gamma)| &= |P^* + P^*(\gamma) - P^*(\gamma) + D_\epsilon^*(\gamma) - D_\epsilon^*(\gamma) - D_{\epsilon, N, \mathcal{E}_{train}}^*(\gamma)| \\ &\leq |P^* - P^*(\gamma)| + |P^*(\gamma) - D_\epsilon^*(\gamma)| + |D_\epsilon^*(\gamma) - D_{\epsilon, N, \mathcal{E}_{train}}^*(\gamma)| \\ &\leq L\gamma + \epsilon t(1 + \|\tau_{pert}^*\|_1) + 2H \sqrt{\frac{1}{N} \left[1 + \log\left(\frac{4(2N)^{d_{VC}}}{\rho}\right) \right]} \end{aligned}$$

□

C.2 More Experimental Results

To further assess the classification performance of our model, we also evaluate the F1 score on TWITCH and FB-100, both of which contain two types of labels. In Table 8 and Table 7, we show the results for the F1 score on TWITCH and FB-100. In comparison to all baselines, our approach exhibits a significant improvement in average F1 scores. From a comprehensive perspective, the EERM and the GroupDRO both rank second only to ours in terms of classification performance. Moreover, they exhibit favorable performance compared to other methods across multiple datasets.

Table 6: Test accuracy (%) on TWITCH where we compare different configurations of training graphs.

Methods	ENGB	ES	DE	FR	PTBR	RU	TW	Avg
EERM	45.7 ± 0.2	<u>70.7 ± 0.2</u>	50.0 ± 1.8	58.2 ± 4.4	65.3 ± 0.0	72.7 ± 3.8	<u>60.7 ± 0.0</u>	60.5
ERM	45.6 ± 0.0	70.6 ± 0.1	40.2 ± 1.3	<u>63.0 ± 0.1</u>	65.0 ± 0.1	66.3 ± 8.5	58.9 ± 2.9	58.5
IRM	42.4 ± 0.4	63.1 ± 2.0	39.0 ± 0.9	49.9 ± 0.1	51.6 ± 0.9	55.3 ± 1.5	46.0 ± 0.7	49.6
DANN	<u>46.5 ± 1</u>	49.5 ± 1.1	36.1 ± 2.1	42.2 ± 1.1	51.8 ± 3.0	48.7 ± 1.6	49.7 ± 1.5	46.6
VREx	39.7 ± 1.0	33.3 ± 4.0	49.2 ± 1.1	47.5 ± 0.8	49.8 ± 3.1	58.7 ± 0.1	49.5 ± 1.4	46.8
SRGNN	40.3 ± 2.0	53.8 ± 1.5	44.9 ± 0.1	48.4 ± 0.4	38.8 ± 2.6	58.8 ± 1.1	44.3 ± 3.7	47.0
Mixup	37.2 ± 1.0	48.7 ± 2.4	48.4 ± 1.5	39.9 ± 2.9	46.9 ± 1.8	59.1 ± 0.8	56.6 ± 0.9	48.1
GroupDRO	45.1 ± 0.9	55.6 ± 0.4	<u>51.0 ± 1.1</u>	53.1 ± 1.2	51.1 ± 2.0	67.1 ± 2.1	47.3 ± 0.4	53.1
GLIDER -C	45.9 ± 0.4	69.9 ± 0.4	50.2 ± 3.1	59.9 ± 3.8	65.0 ± 3.7	<u>74.2 ± 2.1</u>	59.6 ± 2.0	<u>60.7</u>
GLIDER -A	45.4 ± 0.0	70.7 ± 0.0	47.0 ± 2.4	61.9 ± 2.2	<u>65.4 ± 0.0</u>	<u>72.0 ± 2.2</u>	58.4 ± 4.9	60.1
GLIDER	46.7 ± 0.6	70.7 ± 0.7	51.1 ± 2.8	63.1 ± 1.2	65.4 ± 1.2	75.5 ± 1.2	60.8 ± 2.8	61.9

Table 7: F1 score (%) on TWITCH where we compare different configurations of training graphs.

Methods	ENGB	ES	DE	FR	PTBR	RU	TW	Avg
EERM	34.6 ± 2.0	60.4 ± 2.2	53.2 ± 1.9	51.0 ± 2.0	52.0 ± 0.4	65.9 ± 0.7	49.2 ± 2.1	52.3
ERM	40.8 ± 0.1	59.9 ± 0.0	40.1 ± 0.9	57.2 ± 0.0	53.8 ± 2.1	54.1 ± 3.1	45.2 ± 1.6	50.1
IRM	39.9 ± 2.2	<u>61.0 ± 0.5</u>	38.9 ± 0.0	47.2 ± 1.8	45.2 ± 2.2	50.3 ± 2.6	45.0 ± 1.2	46.8
DANN	40.1 ± 0.9	42.3 ± 0.1	35.9 ± 2.1	43.2 ± 2.1	49.6 ± 1.0	47.9 ± 1.2	48.7 ± 2.0	43.9
VREx	39.8 ± 1.0	35.3 ± 1.2	45.7 ± 2.1	46.4 ± 0.7	47.6 ± 2.0	54.3 ± 1.8	49.1 ± 2.3	45.5
SRGNN	40.8 ± 1.0	52.7 ± 3.0	42.7 ± 0.6	48.7 ± 0.1	35.2 ± 2.4	56.0 ± 2.3	45.0 ± 0.9	45.9
Mixup	38.4 ± 0.9	47.9 ± 0.4	47.1 ± 2.0	38.7 ± 1.0	45.5 ± 2.0	57.6 ± 0.6	53.1 ± 2.1	46.9
GroupDRO	<u>46.0 ± 0.1</u>	53.0 ± 1.9	50.7 ± 2.0	52.2 ± 0.9	51.3 ± 2.8	60.4 ± 1.8	46.9 ± 0.7	51.5
GLIDER-C	35.1 ± 1.2	58.5 ± 1.1	50.0 ± 1.0	54.2 ± 1.0	56.6 ± 1.9	58.4 ± 1.3	49.0 ± 0.6	51.7
GLIDER-A	35.7 ± 0.9	59.1 ± 1.5	50.2 ± 0.8	54.0 ± 1.3	<u>59.7 ± 2.2</u>	62.9 ± 1.7	48.8 ± 1.5	<u>52.9</u>
GLIDER	46.0 ± 3.3	61.2 ± 2.6	<u>51.9 ± 2.2</u>	<u>55.1 ± 2.2</u>	60.0 ± 3.6	<u>64.9 ± 3.9</u>	<u>49.3 ± 2.1</u>	55.0

Table 8: F1 score (%) on FB-100 where we compare different configurations of training graphs.

Methods	Hopkins + Caltech + Amherst				Bingham + Duke + Princeton				WashU + Brandeis+ Carnegie			
	Penn	Brown	Texas	Avg	Penn	Brown	Texas	Avg	Penn	Brown	Texas	Avg
EERM	48.6 ± 1.1	47.4 ± 3.1	50.0 ± 2.7	48.6	44.3 ± 2.6	39.8 ± 7.0	48.2 ± 8.6	44.1	51.4 ± 1.8	46.0 ± 2.8	49.4 ± 2.1	48.9
ERM	46.8 ± 2.9	<u>49.1 ± 0.0</u>	51.4 ± 2.1	49.1	37.4 ± 3.4	30.2 ± 1.4	36.9 ± 2.0	34.8	53.1 ± 2.8	43.6 ± 4.8	46.5 ± 1.5	47.7
IRM	44.4 ± 0.1	<u>40.8 ± 1.0</u>	37.4 ± 1.2	40.9	32.1 ± 0.1	30.3 ± 1.4	36.9 ± 1.0	33.1	39.9 ± 1.1	42.8 ± 1.8	41.4 ± 1.8	41.4
DANN	40.5 ± 0.2	41.4 ± 1.2	43.2 ± 2.1	41.7	39.6 ± 0.2	42.8 ± 0.8	42.9 ± 3.0	41.8	41.6 ± 0.7	42.9 ± 1.2	43.0 ± 1.1	42.5
VREx	40.8 ± 2.2	48.5 ± 1.0	45.6 ± 2.1	44.7	41.4 ± 2.0	46.9 ± 2.1	46.8 ± 2.8	45.0	42.8 ± 0.9	49.3 ± 1.0	46.7 ± 0.7	46.3
SRGNN	38.3 ± 0.7	40.0 ± 0.9	44.4 ± 1.6	40.9	39.5 ± 0.6	41.8 ± 0.7	45.3 ± 1.7	42.2	40.5 ± 3.2	41.1 ± 2.6	45.0 ± 0.3	42.2
Mixup	48.2 ± 2.0	43.2 ± 0.1	47.8 ± 0.8	46.4	<u>44.9 ± 1.0</u>	44.6 ± 0.7	48.7 ± 0.5	46.1	50.2 ± 2.0	45.5 ± 0.1	49.5 ± 1.2	48.4
GroupDRO	46.5 ± 0.1	47.5 ± 2.0	48.3 ± 1.0	47.4	<u>44.8 ± 0.3</u>	<u>46.9 ± 2.0</u>	48.8 ± 2.7	<u>46.8</u>	49.9 ± 0.4	48.7 ± 2.1	<u>50.5 ± 0.2</u>	49.7
GLIDER-C	48.3 ± 1.6	48.7 ± 0.6	49.6 ± 0.2	48.9	44.8 ± 2.1	45.7 ± 0.7	50.0 ± 0.3	46.8	51.5 ± 1.0	48.3 ± 0.7	50.2 ± 1.3	50.0
GLIDER-A	<u>48.9 ± 1.0</u>	49.1 ± 0.7	50.9 ± 1.3	<u>49.6</u>	44.1 ± 2.0	46.3 ± 0.5	49.8 ± 1.7	46.7	51.2 ± 1.3	<u>50.1 ± 0.9</u>	50.5 ± 1.6	<u>50.6</u>
GLIDER	49.4 ± 2.0	49.8 ± 1.5	51.8 ± 2.8	51.3	45.0 ± 2.1	47.5 ± 1.0	51.9 ± 1.9	48.1	<u>52.9 ± 2.1</u>	50.8 ± 1.9	51.0 ± 0.8	51.6